ELSEVIER

Journal of Nuclear Materials 297 (2001) 138–148

journal of nuclear materials

www.elsevier.com/locate/jnucmat

Effects of carbide precipitation on the strength and Charpy impact properties of low carbon Mn–Ni–Mo bainitic steels

Young-Roc Im [a,*], Yong Jun Oh [b], Byeong-Joo Lee [c], Jun Hwa Hong [b], Hu-Chul Lee [a]

[a] *School of Materials Science and Engineering, College of Engineering, Seoul National University, Seoul 151-742, South Korea*
[b] *Korea Atomic Energy Research Institute, Taejon 305-353, South Korea*
[c] *Korea Research Institute of Standards and Science, Taejon 305-600, South Korea*

Received 24 July 2000; accepted 4 May 2001

Abstract

The effects of carbide precipitation on the strength and Charpy impact properties of tempered bainitic Mn–Ni–Mo steels have been investigated. An attempt has also been made to modify the microstructure of the steels in order to improve the Charpy properties, by controlling the alloy composition being guided by thermodynamic calculations of phase equilibria. Coarse rod type or agglomerated spherical type cementite particles in inter-lath region were considered to be mostly detrimental to Charpy impact properties. By reducing the precipitation of cementite through decreasing carbon content and/or by substituting it into fine M_2C carbides through increasing the molybdenum content, DBTT could be lowered significantly. Further decrease of DBTT could be achieved by substituting part of manganese content by nickel. Yield strength of tested alloys could be maintained at the level of a reference 0.2 wt% carbon alloy in spite of the significant reduction in carbon content, mainly by the increase in the precipitation of fine M_2C type carbides with increased molybdenum content.

PACS: 81.70.Bt; 81.40.Cd; 81.30.–t

1. Introduction

Nuclear pressure vessels operate under relatively severe environment of elevated temperature, high pressure and neutron bombardment. A good combination of strength, toughness, weldability and high resistance to neutron irradiation are required for the materials. Several grades of low carbon bainitic steels have been developed and utilized for decades as nuclear pressure vessel materials. Among these, quench-and-tempered Mn–Ni–Mo steel is one of the mostly accepted nuclear pressure vessel materials. Many investigations on the strength and toughness [1–3], irradiation damage [4–8], under-clad cracking [1,9,10], and production and thermo-mechanical treatment conditions [7,11–13] for this steel have been carried out. Typical thermo-mechanical treatment cycle for these steels includes forging into a large ring, normalizing, austenitizing, quenching and tempering treatment, welding, and post weld heat treatment (PWHT). Since the major volume of forged ring transforms into a vulnerable upper bainite structure during quenching, achievement of good toughness is one of the most serious issues in processing of this steel. Furthermore, due to neutron irradiation, the ductile–brittle transition temperature (DBTT) rises and the Charpy absorbed energy decreases, continuously during service [5,6]. Therefore, attaining good Charpy properties prior to service is one of the utmost designing goals for nuclear structural materials. In quench and tempered bainitic steels, tensile and Charpy properties of alloys are strongly dependent on the precipitation of carbides, which can be controlled by the alloy composition. But detailed information on the effects of alloy compositions

* Corresponding author. Tel.: +82-2 880 7099; fax: +82-2 882 7745.
E-mail address: everg@plaza1.snu.ac.kr (Y.-R. Im).

0022-3115/01/$ - see front matter
PII: S0022-3115(01)00610-9

on the precipitation of carbides and properties of alloys are still lacking in most of bainitic steels.

The purpose of the present work is to investigate the effects of carbide precipitation on tensile and Charpy impact properties of tempered bainitic Mn–Ni–Mo steels. In order to improve the Charpy properties, the microstructure, particularly the precipitation of carbides, of the steels was modified by the control of alloy composition being guided by CALPHAD [14] type thermodynamic calculations of phase equilibria.

2. Experimental procedure

2.1. Materials and heat treatments

Chemical compositions of the steels examined in this study are listed in Table 1 and compared with ASME specifications for SA508 III steel, one of the typical Mn–Ni–Mo nuclear pressure vessel steels. A laboratory alloy with a typical composition of the SA508 III steel was prepared as a reference alloy (labeled as 'S'). It was intended to reduce the precipitation of cementite, particularly the rod type inter-lath cementite, by decreasing carbon content. It was also intended to make the cementite precipitates to be substituted by M_2C type carbides by increasing molybdenum content. Therefore, many of the other laboratory alloys have lower carbon content and/or higher molybdenum content than the reference alloy, while chromium and silicon contents were kept more or less constant. To compensate the probable decrease of hardenability due to the decrease of carbon content, the amount of substitutional alloying elements, Mo, Mn and Ni, were generally increased. In some alloys, part of manganese content was substituted by nickel.

All alloys were prepared by vacuum induction melting as ingots of 25–50 Kg and then forged into plates of 35 mm in thickness. Heat treatment schedule of plates is organized to duplicate the manufacturing conditions of nuclear pressure vessel. A typical heat treatment of plates includes normalizing at 1200°C, austenitizing at 900°C, cooling at the rate of 20°C/min and tempering at 660°C for 10 h. Austenitizing condition was controlled to produce a constant prior austenite grain size of 30 μm to exclude grain size effects on the mechanical properties of these steels. The cooling rate of 20°C/min was selected in accordance with the reported value measured from 1/4t thickness position of modern nuclear pressure vessel.

2.2. Microstructural investigation

Microstructural observations at low magnification were conducted using optical and JSM-5600 scanning electron microscopes. Metallographic specimens for these observations were prepared by grinding and polishing to final 0.3 μm powder then etched in 2% Nital or 1:1 mixed solution of Nital and Picral. To investigate overall distribution of carbides and to analyze individual carbide particles in detail, carbon extraction replica technique had been employed. Replicas were prepared from the specimens that had been polished and etched. The specimens were then carbon coated, and the carbon films were extracted in the solution of 10–15% perchloric acid in methanol at 5 V. Carbon extraction replicas and conventional thin foil specimens were examined using JEM-200CX transmission electron microscope.

2.3. Thermodynamic calculation

The phase equilibria of tested alloys at tempering temperature were calculated by CALPHAD method. In the CALPHAD method, the Gibbs energies of individual phases are described using thermodynamic models. Then, the calculations of phase equilibria are performed based on the minimum-of-Gibbs-energy criterion, for example, the Hillert's equilibrium condition [15]. By this method, the equilibrium amounts and compositions of

Table 1
Chemical composition of tested alloys (wt%)

Alloy	C	Mn	Ni	Mo	Cr	Si	Al
SA508 III	0.25	1.20	0.40	0.45	0.25	0.15	–
(ASME)	Max	~1.50	~1.00	~0.60	Max	~0.40	–
S	0.20	1.37	0.91	0.48	0.15	0.21	0.030
A	0.20	0.68	1.88	0.50	0.15	0.20	0.030
B	0.15	1.38	1.00	0.49	0.16	0.15	0.002
C	0.16	1.51	1.00	0.78	0.16	0.17	0.006
D	0.16	1.01	1.48	0.49	0.15	0.21	0.021
E	0.10	0.70	1.48	0.76	0.15	0.21	0.023
F	0.11	0.70	1.40	0.91	0.13	0.19	0.002
G	0.10	0.70	1.90	1.51	0.15	0.20	0.034
H	0.06	1.48	0.97	0.90	0.14	0.19	0.013
I	0.06	1.00	1.41	0.91	0.14	0.19	0.008
J	0.05	0.50	3.45	0.98	0.15	0.20	0.045

individual phases are calculated under a given temperature and overall composition. More details on the thermodynamic model parameters have been published in [16]. Mole fraction of carbides calculated by CALPHAD method was converted to volume fraction considering the density of carbides.

2.4. Mechanical testing

Tensile properties of alloys were evaluated using 10 ton capacity testing machine (Instron 5582). Yield strength was determined by 0.2% strain offset stress, or by lower yield stress in case of the occurrence of yield drop. Impact transition curves were obtained using standard Charpy V-notched specimens of T–L orientation. Impact tests were conducted using Tinius Olsen impact testing machine of maximum capacity 409 J in a temperature range from −150°C to 200°C. The DBTTs were determined from fitted Charpy curves as the temperature corresponding to the mean value of upper and lower shelf energies.

3. Results

3.1. Microstructure of low carbon Mn–Ni–Mo bainitic steel

Due to the mass effect, the major part of pressure vessel transforms into bainitic structure after quenching. Typical microstructural features of the SA508 III pressure vessel steels are presented in Fig. 1, which shows tempered upper bainite structure. Cementite particles of long rod shape are distributed in regions between bainitic ferrite laths. This inter-lath region is formed in the later stages of bainite transformation, by the enrichment of ejected carbon from surrounding bainitic ferrite laths. Higher magnification TEM micrograph reveals that inter-lath region is an aggregate of long rod (about 0.3 μm thick and 3 μm long) type and spherical (about 0.2 μm in size) type cementite particles. In bainitic ferrite laths, fine needle-like carbides (about 0.02 μm thick and 0.3 μm long) identified as molybdenum-rich M_2C type carbides are densely distributed. This M_2C carbide precipitates mainly during the tempering period.

It has been reported that particles of higher aspect ratio are more vulnerable to fracture than spherical ones [2,17]. Therefore, the rod type cementite particles present in inter-lath region were expected to be the primary source of fracture in this steel. Tensile tests at ductile fracture region using round-notched cylindrical specimens revealed that rod type cementite is a major void source in this type of steels [18] (Fig. 2). Fig. 3 shows the microcracks encompassing cementite-crowded inter-lath regions in double sharp-notched cylindrical tensile specimens fractured in a brittle lower shelf temperature

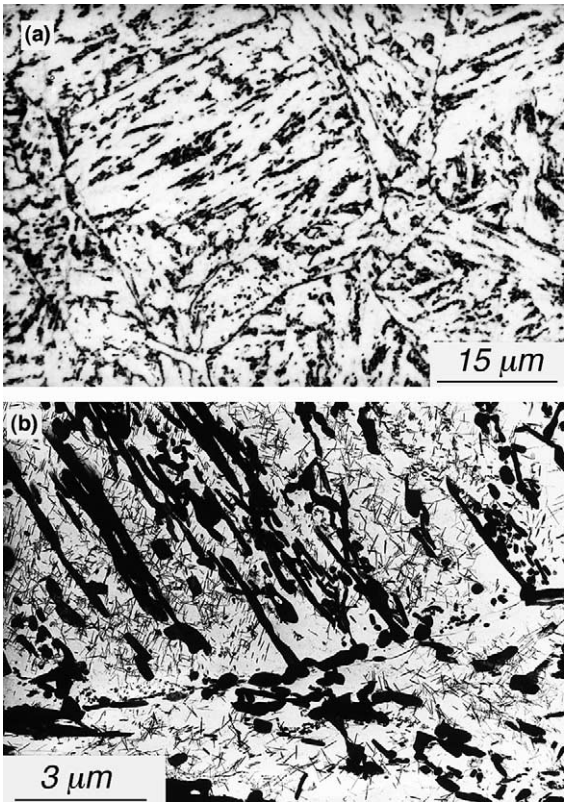

Fig. 1. Typical microstructures of SA508 III steels. (a) Optical micrograph; (b) Transmission electron micrograph (replica).

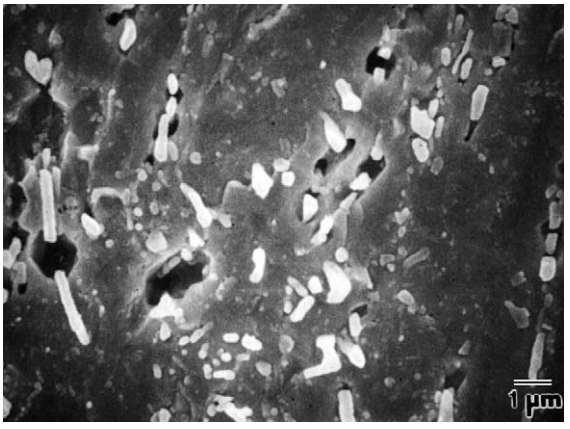

Fig. 2. Void initiation at rod type cementite [18].

region. The micrograph is taken from the unbroken notch section. These micrographs clearly show that the initiation of fracture in this steel is associated with carbides, mostly cementite particles. Based on these observations, the reduction of inter-lath cementite was aimed as a main goal of alloy design to improve the toughness of this steel.

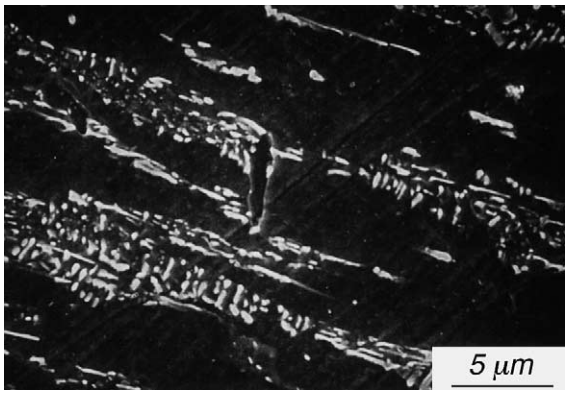

Fig. 3. SEM micrographs showing inter-lath microcracks.

3.2. Precipitation of carbides

The changes of microstructure with carbon contents at as-quenched condition are shown in Fig. 4. Inter-lath cementite precipitation (black area in Fig. 4) is significantly reduced with decreasing carbon contents, as expected. Granular bainitic type structure with M/A (martensite/retained austenite) phase are also observed in lower carbon (0.10 and 0.05 wt%) alloys. Typical tempered microstructures at each carbon grade are presented in Fig. 5. Higher carbon (0.20 and 0.15 wt%) alloys show tempered upper bainitic structures but lower carbon alloys demonstrate a unique microstructure in according to further decrease in cementite particles during tempering treatment. Since the molybdenum contents are higher in lower carbon alloys to compensate the loss of strength and hardenability, most of cementite carbides are substituted into M_2C type or other molybdenum-rich carbides during tempering. Bainitic characteristics cannot be seen in optical micrographs of Figs. 5(c) and (d), which means inter-lath cementite precipitates are mostly substituted into much finer M_2C carbides.

Equilibrium fractions of carbides at tempering temperature were calculated and listed in Table 2. Alloys may not reach full equilibrium after tempering for 10 h at 660°C, but we believe they are very near to it and thermodynamic calculation well represents real microstructure. For example, in high molybdenum alloys, cementite particles formed during bainitic transformation are mostly substituted to M_2C type carbides after tempering. Only a few cementite particles were poradically observed at grain boundaries. In the reference alloy (S, 0.2 wt% C), equilibrium weight fraction of cementite is calculated to be 2.61%. Cementite fraction decreases approximately 0.9% by 0.05 wt% reduction of carbon content without an increase in molybdenum content.

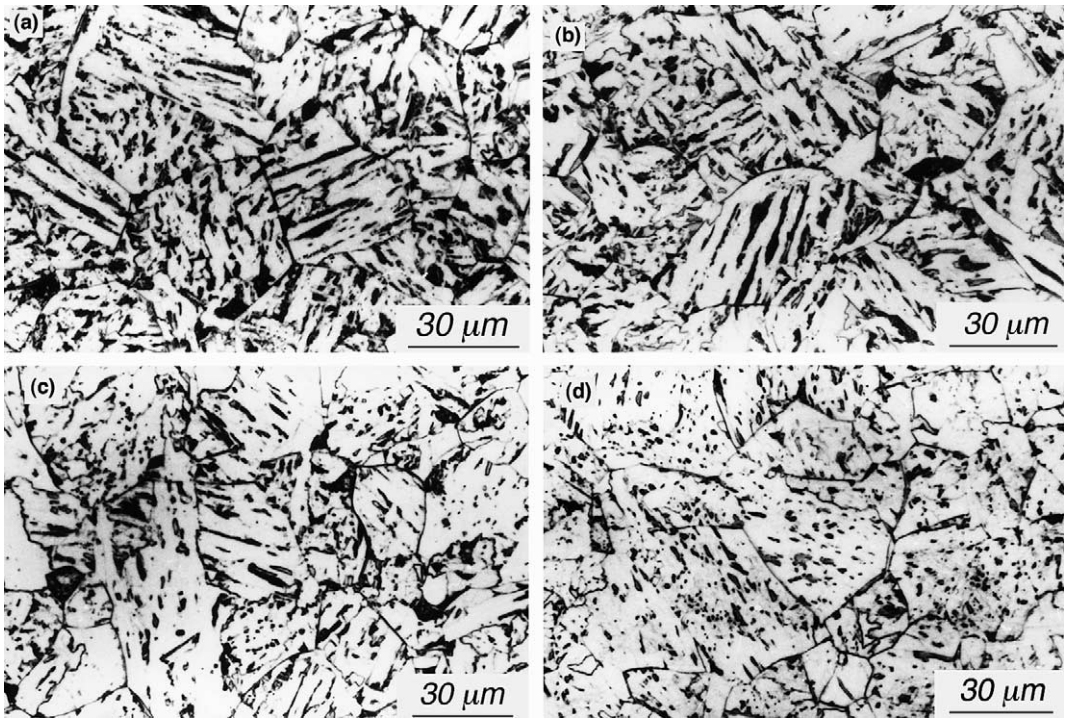

Fig. 4. Change of microstructures with carbon content (as quenched). (a) 0.20 wt% carbon alloy (A); (b) 0.15 wt% carbon alloy (D); (c) 0.10 wt% carbon alloy (E); (d) 0.05 wt% carbon alloy (J).

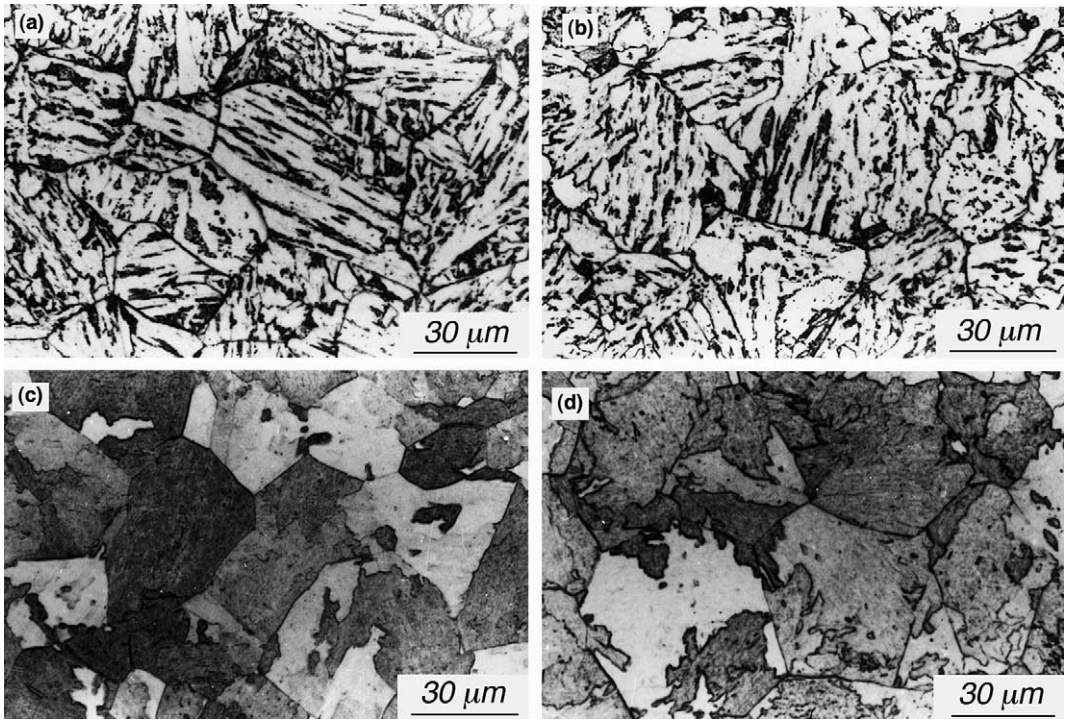

Fig. 5. Change of microstructures with carbon content (tempered). (a) 0.20 wt% carbon alloy (A); (b) 0.15 wt% carbon alloy (D); (c) 0.10 wt% carbon alloy (G); (d) 0.05 wt% carbon alloy (I).

Table 2
Equilibrium weight fraction of cementite and M_2C carbides at tempering temperature

Alloy	Precipitates (wt%, 650°C)		
	M_2C	Cementite	Others
S	0.33	2.61	
A	0.34	2.56	
B	0.35	1.70	
C	0.70	1.40	
D	0.34	1.92	
E	0.67	0.79	
F	0.84	0.77	
G	1.51	0	
H	0.81	0	
I	0.83	0	
J	1.67	0	γ 8.3

Weight fraction of M_2C type carbide is calculated to be 0.33% in the reference alloy and increase with increasing molybdenum content up to 1.51% in the alloy with 0.10 wt% carbon and 1.5 wt% molybdenum. Thermodynamic calculations predict no cementite precipitations in alloy G, H, I, and J. Precipitation of inter-lath rod-like and densely distributed globular cementite particles was not observable in 0.10 wt% carbon and 1.5 wt% molybdenum alloy (alloy G, Fig. 5(c)) and also in 0.05 wt% carbon and 1.0 wt% molybdenum alloy (alloy I, Fig. 5(d)).

3.3. Mechanical properties of alloys

Alloys with varying carbon levels, 0.20, 0.15, 0.10 and 0.05 wt% were examined in the present work. The reduction in carbon content will inevitably decrease the strength and hardenability of the alloys. To compensate these losses, the concentration of substitutional alloying elements in lower carbon alloys was increased. The mechanical properties of tested alloys are given in Table 3. The strength level can be maintained at the almost same or higher level of the reference alloy (S) in all tested alloys, in spite of the significant reduction in carbon content in some alloys. Precipitation hardening by fine M_2C carbides in addition to the lowering of bainite start (Bs) temperature due to the increased nickel and manganese addition is proved to be sufficient to maintain the yield and tensile strength levels. Without sacrificing the strength level of the reference alloy, DBTT can be lowered significantly by the reduction of cementite precipitation. Further decrease in DBTT is achieved by the substitution of nickel for manganese.

The changes of impact properties with alloying elements investigated in this work are summarized below.

Table 3
Tensile and Charpy impact properties of tested Mn–Ni–Mo alloys

Alloy	Tensile properties (MPa)		Impact properties	
	YS	TS	USE (J)	DBTT (°C)
S	462	601	272	+8
A	451	586	227	−24
B	444	559	331	−20
C	496	625	303	−2
D	468	582	241	−37
E	479	603	218	−29
F	500	606	393	−33
G	607	733	249	−55
H	440	580	415	−60
I	461	570	404	−84
J	483	615	408	−83

3.4. Effect of carbon

The improvements of impact properties with decreasing carbon contents is demonstrated in Fig. 6. DBTT is lowered and the upper shelf energy is increased with decreasing carbon content. The brittle-to-ductile transition of a BCC alloy is accompanied by a change in fracture mechanism from cleavage to void coalescence, and DBTT of an alloy can be quantitatively interpreted as a result of the competition between the flow stress and cleavage fracture stress of the alloy. DBTT of an alloy will be shifted to lower temperature if cleavage fracture stress is increased or flow stress is decreased. Since the flow stress of tested alloys are maintained at the almost same or higher level of the reference alloy, the decrease of DBTT with carbon reduction can be explained by the increase of cleavage fracture stress. The width of dense cementite inter-lath regions, which was considered to be primary fracture sources, decreases with reduction in carbon content, and the cleavage fracture stress will rise with the decrease of these Griffith type crack length (Fig. 3). In general, upper shelf energy increases with reducing carbon content except in alloys of very high strength, for example, alloy G. Upper shelf energy is determined by the plastic energy absorbed during fracture process of void nucleation and coalescence. Compared to other alloys, alloy G has very high yield strength due to its high density of Mo_2C precipitates. It is believed that plastic deformation is limited due to these precipitates.

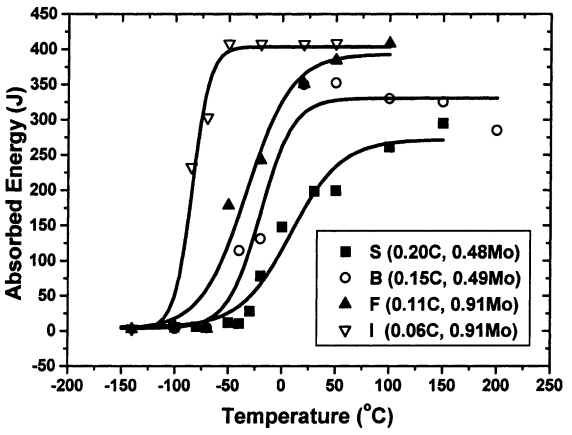

Fig. 6. Change of Charpy impact properties with carbon content.

3.5. Effects of molybdenum

Molybdenum is known to suppress polygonal ferrite transformation and increases the strength of tempered alloys through precipitation of very fine M_2C carbides. Increasing molybdenum content can be an efficient way to achieve higher strength and better hardenability. CALPHAD calculation shows approximately 0.1% increase in the weight fraction of M_2C carbides with the 0.1 wt% increase in molybdenum contents in the alloys.

The effect of molybdenum on DBTT is appeared to vary with carbon contents. In lower carbon (0.10 and 0.05 wt% carbon) alloys, the increase in molybdenum concentration lowers DBTT in spite of the increase in yield strength. But, in higher carbon alloys, the increase in molybdenum concentration turned out to have adverse effect on toughness, i.e., raise the transition temperature. The effects of molybdenum on the DBTT of 0.10 and 0.15 wt% carbon alloys are compared in Fig. 7. In 0.15 wt% carbon steels, addition of molybdenum increases DBTT of the alloys as well as its yield strength. But, in 0.10 wt% carbon steels, addition of molybdenum resulted in the decrease of DBTT in spite of dramatic increase in its yield strength. This result could be explained by the substitution of detrimental cementite particles to fine M_2C carbides by the addition of molybdenum. As shown in Fig. 3, cleavage fracture is initiated from micro-cracks in dense cementite inter-lath regions. In low carbon high molybdenum steels, the dense cementite area will be effectively removed after tempering as shown in Figs. 5(c) and (d). Cleavage fracture stress will be increased, resulting in the decrease in DBTT. In higher carbon alloys, initial volume fraction of cementite is high and the level of molybdenum content is not enough to substitute cementite extensively. Large addition of molybdenum for higher carbon alloys to the extent that extensive substitution of cementite to M_2C occurs was not attempted because it will end up with too much higher strength.

3.6. Effect of substitution of nickel for manganese

Increasing the manganese and/or nickel contents of alloys can be an effective way to compensate the loss of strength and hardenability due to the reduction in

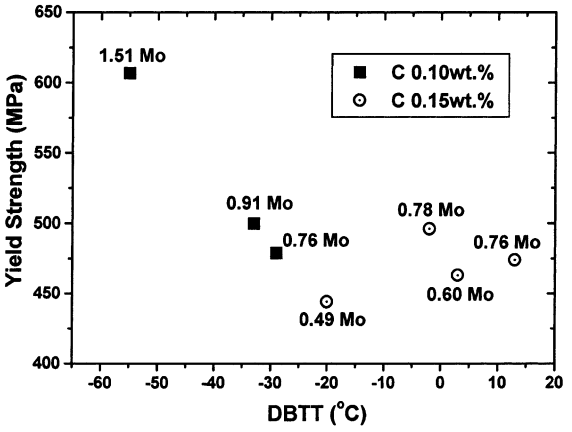

Fig. 7. The relation between DBTT and yield strength for 0.10 and 0.15 wt% carbon alloys.

carbon content. Nickel is also known to be beneficial to DBTT [1,19,20]. But, if total content of manganese and nickel exceeds certain level, austenite phase forms during tempering and resulted in M/A (martensite plus retained austenite) phase upon cooling to room temperature. This could result in very poor toughness. In this experiment, total content of these austenite stabilizers was limited to avoid the precipitation of M/A phase and, within the limit, the ratio of nickel to manganese was increased. The improvement of DBTT with the substitution of nickel for manganese is demonstrated in Fig. 8. 'A' alloy having same total composition with the reference alloy 'S' except the relative contents of manganese and nickel shows decrease in DBTT by about 30°C. Similar improvement is achieved in alloy 'I'. The differences in microstructure with the substitution of nickel for manganese are not significant in spite of the significant differences in impact properties. Enhanced cross

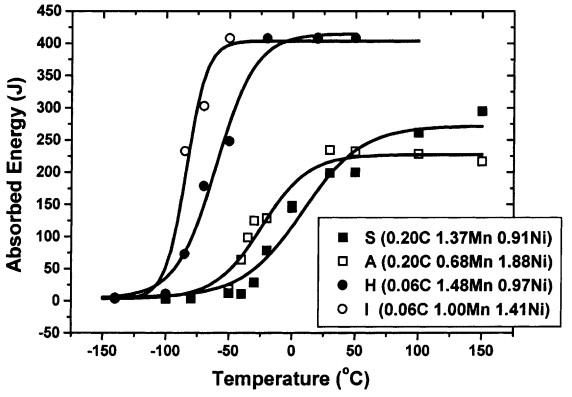

Fig. 8. Change of Charpy impact properties with nickel substitution for manganese.

slip of dislocations in higher nickel alloys is suggested in the [20,21].

4. Discussion

4.1. Tensile properties and carbide precipitation in Mn–Ni–Mo alloys

The major goal of this experiment is to improve the impact property of the alloys without sacrificing their yield strength. Inter-lath cementite precipitation was reduced by the reduction of carbon content or by the substitution to M_2C type carbide during annealing. Yield strength of the tested alloys varies from 444 to 607 MPa, and high yield strength was achieved in high molybdenum alloys even in the alloys of 0.10 and 0.05 wt% carbon. The microstructural factors affecting the strength of bainitic steels can be:

(a) Slip distance, which is related to grain, packet or lath size;
(b) Dislocation density;
(c) Solid solution hardening by substitutional and interstitial elements; and
(d) Precipitation hardening by carbides.

In present investigation, the prior austenite grain sizes are controlled to 30 μm level in all alloys and the packet sizes are about 1/3–1/2 of the grain sizes regardless of the carbon content. The influence of lath width on the strength of bainitic steels has also been discussed in literatures [22,23]. The lath width can vary by the change in bainite transformation temperature, which is mainly determined by the alloy composition. In the tested alloys, variations in Bs temperatures are limited within ±15°C and the variation in lath size was limited within 0.2 μm in all alloys. Dislocation density in fresh bainite can also vary with bainite transformation temperature. However, after 10 h of tempering at 660°C, dislocation densities in tempered alloys are very low and the differences in contributions from varying dislocation densities in different alloys would not be significant. Another contribution to the alloy strength can be expected from solid solution hardening. But total contents of manganese plus nickel are kept more or less constant near 2.5 wt% and differences in contribution to the alloy strength among these elements will not be significant. Molybdenum is also a potent solid solution hardening element. But, in tested alloys, molybdenum will precipitate out as M_2C carbides and its solid solution effect will not be significant.

The major contributing factor that differs between alloys is expected to be from the precipitation hardening by carbides. The hardening effect of M_2C carbide is demonstrated in Fig. 9, which shows the relationship between the yield strength of tested alloys and calculated equilibrium volume fraction of M_2C carbide. Linked

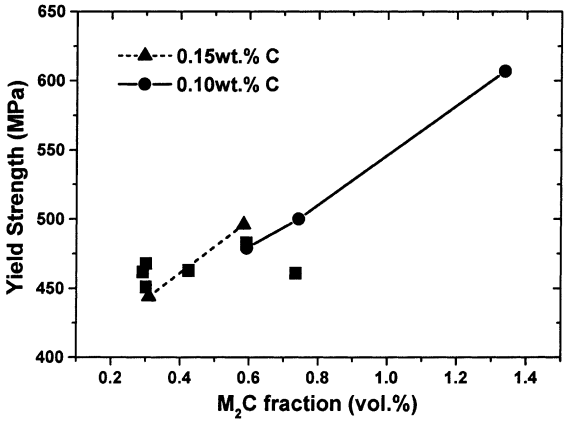

Fig. 9. The variation of yield strength of tempered alloys with calculated equilibrium volume fraction of M_2C.

data points in Fig. 9 represent the increase of yield strength with increasing molybdenum content when chemistry of other alloying elements including carbon are nearly identical. Approximate precipitation hardening effect of this carbide is 15 MPa per 0.1 vol.% of carbide, which is equivalent to about 0.1 wt% of molybdenum. For 0.10 wt% carbon alloys, the strength level of the reference alloy could be achieved in 0.8 wt% of molybdenum alloy and yield strength of as high as 600 MPa, which was 150 MPa higher than that of the reference alloy, was obtained by the addition of 1.5 wt% of molybdenum.

The precipitation hardening effect of M_2C carbide can be interpreted by Orowan [24] type relationship (Eq. (1)) as a function of the mean center-to-center distance of plate-like precipitates [25]. (Eq. (2))

$$\Delta\sigma_y = 3Gb/L, \tag{1}$$

$$L = (\pi D^2/\sqrt{6}f)^{1/2}, \tag{2}$$

where f is the volume fraction of M_2C carbide and D is the diameter of the precipitates. After 10 h of tempering, the average diameter of the M_2C carbides was about 0.02 μm. Using this value, Eq. (1) can be written as follows:

$$\Delta\sigma_y = 2660^* f_{M_2C}^{1/2} \text{ (MPa)}. \tag{3}$$

Consequently, the yield strength of tested alloys can be expressed as follows by combining the precipitation hardening effect of M_2C carbides and a constant which sums up the possible contributions from lattice friction, solid solution, grain size, lath size, and dislocation density.

$$\sigma_{ys} = 290 + 2660^* f_{M_2C}^{1/2}. \tag{4}$$

In Fig. 10, calculated yield strengths are compared with the measured yield strengths of tested alloys. The correlation is fairly good, which means that the yield strength variations in tested alloys can be explained by the precipitation hardening of M_2C carbides. It can be said that the precipitation hardening of M_2C precipitates does the major role in the compensation of the yield strength loss due to the carbon reduction in tested alloys. The strength level of the reference alloy can be achieved at the same or higher levels in spite of the significant reduction in carbon content by increasing the precipitation of M_2C carbide. The hardenability of the alloys can also be improved by the increase in substitutional alloying elements, Mn, Ni and Mo.

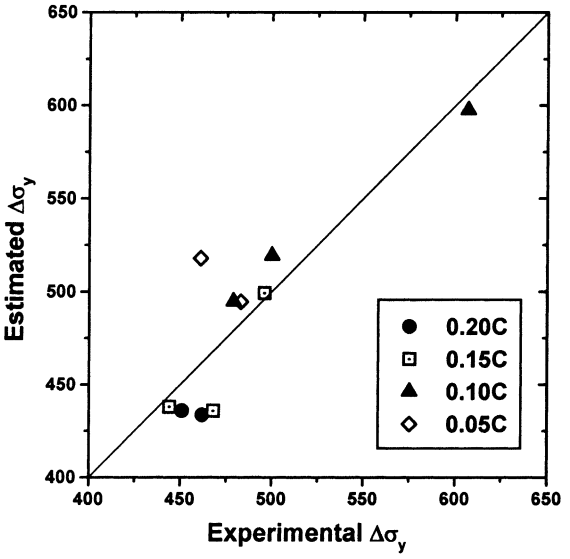

Fig. 10. Comparison between calculated and measured yield strengths of tested alloys.

4.2. DBTT and carbide precipitation in Mn–Ni–Mo alloys

The relationships between DBTT and calculated cementite volume fractions are shown in Fig. 11. In general, DBTT lowers with the reduction in cementite volume fraction. The vertical scatters shown as arrows in Fig. 11 represent the DBTT changes with manganese/nickel substitution at similar cementite volume fractions. Decrease in DBTT with decreasing cementite fraction is believed to be due to the reduction in the precipitation of coarse rod type and spherical type cementite particles, which are considered as major detrimental microstructural features in upper bainitic steels. Reduction of the precipitation of cementite is achieved either by the reduction of carbon content and/or by the substitution to fine M_2C type carbide by increasing molybdenum content of the alloy. Sub-micron sized M_2C type carbides are not likely to initiate fracture, even though it strongly affects the yield strength of the alloys. For 0.10 wt%

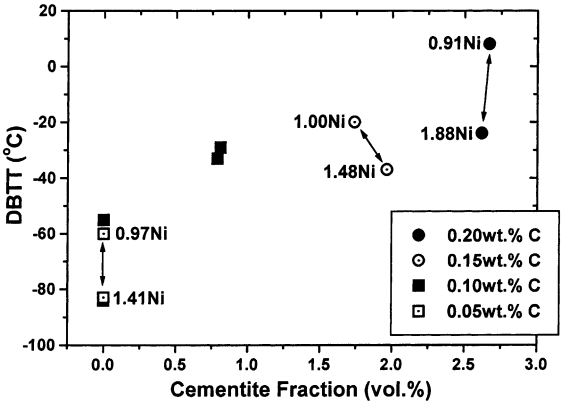

Fig. 11. The relation between DBTT and calculated equilibrium volume fraction of cementite.

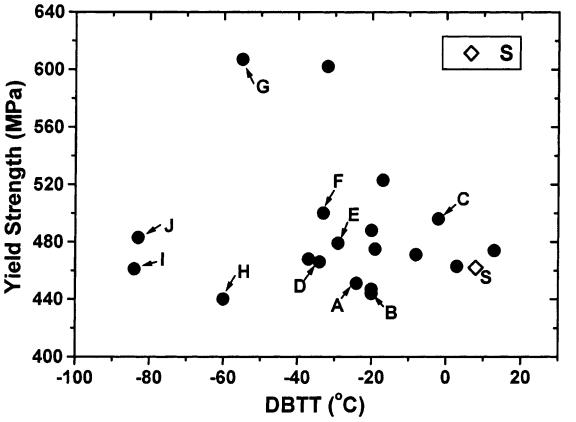

Fig. 12. Yield strength and DBTT of all tested alloys.

carbon and 1.5 wt% molybdenum alloy 'G', low DBTT (−55°C) was obtained in spite of its very high yield strength level. It was found that increase of molybdenum content is a very effective way to increase yield strength of the alloys without sacrificing its low temperature toughness. By the combination of the reduction in carbon content and the increase in molybdenum content, precipitation of cementite can be completely eliminated and DBTT was successfully suppressed to very low temperatures. In this method, hardenability is compensated by the increase in total substitutional alloying element, Mn, Ni and particularly Mo, content. Further decrease in DBTT is achieved by the substitution of nickel for manganese at corresponding cementite fractions. For 0.05 wt% carbon and 1.0 wt% molybdenum alloy 'I' which has high nickel content and near-zero cementite fraction, DBTT value of −84°C was achieved, the lowest level in this study.

Variations in yield strength and DBTT of all tested alloys are presented altogether in Fig. 12. The yield strength could be maintained at or above the level of the reference alloy (S) in nearly all of the tested alloys, while the DBTT of tested alloys are lowered by nearly 100°C. Directions for the improvement of mechanical properties of this type of bainitic alloys can be suggested as follows: Carbon content should be lowered to improve alloy toughness, and strength and hardenability should be maintained by increasing the substitutional alloy contents. The total amount of manganese and nickel could be increased within the limit to avoid the formation of M/A phase, which can be predicted by thermodynamic calculations, and nickel content should be increased substituting for manganese within this limit. Molybdenum addition to higher carbon alloys requires thorough examination to balance strength and toughness. In this work, toughness deterioration due to additional M_2C precipitation is observed in 0.15–0.20 wt% carbon alloys. For lower carbon alloys, increasing molybdenum contents could be beneficial to DBTT as well as strength and hardenability, through extensive removal of detrimental cementite.

The compositions of lower carbon alloys examined in this study considerably deviate from that of currently used SA508 III alloys for nuclear pressure vessel. For the application for nuclear pressure vessel, other requirements, such as weldability and neutron irradiation characteristics, should also be considered. Stress relief cracking (SRC) occurs during PWHT, which is characterized by intergranular fracture along the prior austenite grain boundaries in coarse-grained regions of the HAZ [1,9,10]. The SRC of reactor pressure vessels is also termed as 'underclad cracking' since it is often associated with the stainless steel cladding for corrosion resistance. Underclad cracking is believed to occur by precipitation strengthening of matrix and the cracking susceptibility increases with increasing carbide formers such as Mo, Cr and Co. Upon heating to elevated temperature, residual stress relaxation occurs along the weakest path, i.e., carbide depleted grain boundaries. Underclad cracking can also occur by the reduced cohesive strength of grain boundary due to the segregation of impurity or intergranular precipitation, or by the liquation cracking due to the dissolution of non-metallic inclusions. It has been reported that the cracking susceptibility of higher chromium pressure vessel steels such as SA508 II and 22NiCrMo37 is low [9], but chromium reduces the precipitation of M_2C according to thermodynamic predictions and consistent tendency was confirmed by observation. An alternate explanation [10] is that chromium retards stress relaxation, which causes increased cracking susceptibility. This explanation implies that the contribution from carbide formers such as molybdenum or cobalt may not be the principal cause of underclad cracking. Among the tested alloys in this work, low carbon high molybdenum alloys are of major

concern with respect to the underclad cracking susceptibility. However, the toughness of higher molybdenum alloys has been greatly improved and the effect of M_2C carbides on underclad cracking is obscure when considering the controversial roll of chromium in SA508 II and 22NiCrMo37 steels and yet to be clarified. Impact property of HAZ of low carbon high molybdenum alloys have been proved satisfactory [18], although the typical underclad cracking test has not been carried out. Fatigue property of low carbon high molybdenum alloys is also a concern for structural application. Reduction of larger and agglomerated cementite particles to smaller M_2C type carbides may be beneficial for fatigue initiation but the effect of larger number of M_2C type carbides on fatigue propagation is yet to be verified.

Nuclear pressure vessels are exposed to neutron irradiation and high resistance to irradiation embrittlement is required for nuclear pressure vessel materials. Copper is a well-known irradiation embrittling agent forming copper-rich precipitates or copper–vacancy clusters. Nickel has been known to have synergetic effect with copper [4] enhancing embrittling effect of copper. Other adverse effects of nickel, such as promoting segregation of phosphorous [7] or formation of microvoid [8] have also been reported. However, reports on the high radiation resistance of high nickel steels can also be found in literatures. Hawthorne [4] reported no increase in radiation damage by the increase of nickel from 0.05 to 0.96 wt% when copper content was very low as 0.05 wt%. Stofanak et al. [6] also reported that 3.5 wt% nickel and 0.05 wt% copper steel, which has similar composition to SA508 class IV, offers very good radiation resistance. But, in 1.2 wt% nickel and 0.2 wt% copper steel, they reported very high radiation damage. Further works are required to clarify the effect of nickel on radiation damage in alloys of relatively high nickel concentration (1.0–3.5 wt%).

In the present work, nickel content in the alloys was increased to improve the low temperature toughness and, for the nuclear service, radiation resistance of these steels has to be confirmed. Neutron radiation hardening behaviors of these high nickel alloys are now under investigation.

5. Conclusions

In an attempt to improve the low temperature impact properties of bainitic Mn–Ni–Mo steels, effects of alloy chemistry on the microstructure, strength and Charpy impact properties were investigated and the results are summarized in the following:

1. Coarse rod type and spherical type cementite particles present in inter-lath region are considered as major detrimental microstructural features to the toughness of this type bainitic alloys.
2. Cementite phase is not stable at tempering temperature (660°C) in low carbon high molybdenum alloys, and can be completely substituted by more stable M_2C type carbides after tempering by the increase in molybdenum content of the alloy.
3. The strength level of the reference alloy can be maintained at the almost same or higher level in nearly all tested alloys in spite of the significant reduction in carbon content down to 0.05 wt%. Precipitation hardening of fine M_2C carbides is proved to be sufficient to maintain the yield and tensile strength levels.
4. DBTT can be lowered by reducing the precipitation of cementite by decreasing carbon content or by substituting it into fine M_2C carbides through increasing molybdenum content. Further lowering of DBTT is achieved by the substitution of nickel for manganese. Lowest DBTT of −84°C and upper shelf energy of 400 J were achieved by the combination of complete removal of cementite and partial substitution of nickel for manganese.
5. CALPHAD type thermodynamic calculation of phase equilibria has been very effective in predicting microstructural constituents in the present alloys and can provide sufficient guidelines for alloy design for further improvement of properties.

Acknowledgements

This work has been carried out as a part of the 'Reactor Pressure Boundary Materials Project' of Korea Atomic Energy Research Institute under the Nuclear R&D Program supported by the Korea Ministry of Science and Technology. The authors would like to thank Professor Kwang Sun Shin of Seoul National University and Professor Sunghak Lee of Pohang University of Science and Technology for their helpful discussions on the fracture behavior of alloys.

References

[1] T.D. Nelson, R.L. Bodnar, J.E. Fielding, in: Proceedings of the 32nd Mechanical Working and Steel Processing, Iron and Steel Society of AIME, Warrendale, PA, 1991, p. 323.
[2] P. Bowen, S.G. Druce, J.F. Knott, Acta Metall. 34 (1986) 1121.
[3] M. Lin, S.S. Hansen, T.D. Nelson, R.B. Focht, in: E.G. Nisbett, A.S. Melilli, (Eds.), Proceedings of the 1996 2nd Symposium on Steel Forgings, ASTM STP 1259, American Society for Testing and Materials, Philadelphia, PA, 1997. p. 33.
[4] J.R. Hawthorne, Nucl. Eng. Des. 89 (1985) 223.
[5] K. Suzuki, J. Nucl. Mater. 108&109 (1982) 443.
[6] R.J. Stofanak, T.J. Poskie, Y.Y. Li, G.L. Wire, in: R.E. Gold, E.P. Simonen (Eds.), Proceedings of the 6th International Symposium on Environmental Degradation

of Materials in Nuclear Power Systems – Water Reactors, The Minerals, Metals, and Materials Society, Warrendale, PA, 1993, p. 757.
[7] A.V. Nikolaeva, Yu.A. Nikolaev, A.M. Kryukov, J. Nucl. Mater. 218 (1994) 85.
[8] G.R. Odette, G.E. Lucas, Radiation Embrittlement of Nuclear Reactor Pressure Vessel Steels, in: L.E. Steele (Ed.), ASTM-STP 909, American Society for Testing and Materials, Philadelphia, PA, 1986, p. 206.
[9] S.G. Druce, B.C. Edwards, Nucl. Energy 19 (1980) 347.
[10] J. Shin, C.J. McMahon Jr., Met. Sci. 18 (1984) 403.
[11] P. Bernabei, L. Callegari, M. Scepi, T. Salinetti, Steel Forgings, in: E.G. Nisbett, A.S. Melilli (Eds.), ASTM STP 903, American Society for Testing and Materials, Philadelphia, PA, 1986, p. 275.
[12] R.M. Boothby, C.A. Hippsley, O.K. Gorton, S.J. Garwood, Nucl. Energy 34 (1995) 229.
[13] B. Chapelle, Nucl. Energy 31 (1992) 417.
[14] L. Kaufman, H. Bernstein, Computer Calculation of Phase Diagrams, Academic, New York, 1970.
[15] M. Hilert, Phys. B 103 (1981) 31.
[16] B.-J. Lee, H.-D. Kim, J.-H. Hong, Metall. Mater. Trans. A 29 (1998) 1441.
[17] H.L. Ewalds, R.J.H. Wanhill, in: Fracture Mechanics, Edwards Arnold Ltd, London, 1984, p. 43.
[18] S. Kim, Y.-R. Im, S. Lee, H.-C. Lee, Y.J. Oh, J.H. Hong, unpublished work.
[19] L.-Å. Norström, O. Vingsbo, Met. Sci. 13 (1979) 677.
[20] W.C. Leslie, in: The Physical Metallurgy of Steels, McGraw-Hill, New York, 1981, p. 302.
[21] U. Hildebrandt, W. Dickenscheid, Acta Metall. 19 (1971) 49.
[22] P. Brozzo, G. Buzzichelli, A. Mascanzoni, M. Mirabile, Met. Sci. 11 (1977) 123.
[23] J.P. Naylor, Metall. Trans. A 10 (1979) 861.
[24] E. Orowan, in: Symposium on Internal Stresses, Institute of Metals, London, 1947, p. 451.
[25] J.W. Martin, in: Precipitation hardening, Butterworth–Heinemann, Oxford, 1998, p. 59.